

1 **Transport pathways of carbon monoxide from Indonesian fire**
2 **pollution to a subtropical high-altitude mountain site in western**
3 **North Pacific**

4 Saginela Ravindra Babu^{1*}, Chang-Feng Ou-Yang¹, Stephen M. Griffith¹, Shantanu Kumar Pani¹,
5 Steven Soon-Kai Kong¹, and Neng-Huei Lin^{1,2*}

6
7 ¹Department of Atmospheric Sciences, National Central University, Taoyuan 32001, Taiwan.

8 ²Center for Environmental Monitoring and Technology, National Central University, Taoyuan
9 32001, Taiwan.

10 Correspondence to: S. Ravindra Babu (baburavindra595@gmail.com) and Neng-Huei Lin
11 (nhlin@cc.ncu.edu.tw).

12 **Abstract:** Dry conditions associated with El Niño and a positive Indian Ocean Dipole (IOD) are
13 known to have caused major fire pollution events and intense carbon emissions over a vast spatial
14 expanse of Indonesia in October 2006 and 2015. During these two events, a substantial increase in
15 carbon monoxide (CO) mixing ratio was detected by in-situ measurements at Lulin Atmospheric
16 Background Station (LABS, 23.47°N 120.87°E, 2,862 m ASL) in Taiwan, the only background
17 station in the subtropical western North Pacific region. Compared to the long-term October mean
18 (2006-2021), CO was elevated by ~47.2 ppb (37.2%) and ~36.7 ppb (28.9%) in October 2006 and
19 2015, respectively. This study delineates plausible pathways for CO transport from Indonesia to
20 LABS using MOPITT CO observations and MERRA-2 reanalysis products (winds and
21 geopotential height (GpH)). Two simultaneously occurring transport pathways were identified: (i)
22 horizontal transport in the free troposphere and (ii) vertical transport through the Hadley
23 circulation (HC). The GpH analysis of both events revealed the presence of a high-pressure
24 anticyclone over the northern part of the South China Sea (SCS), which played an important role
25 in the free tropospheric horizontal transport of CO. In this scenario, CO in the free troposphere is
26 transported on the western edge of the high-pressure system and then driven by subtropical
27 westerlies to LABS. Simultaneously, uplifted CO over Indonesia can enter the HC and transfer to
28 subtropical locations such as LABS. The vertical cross-section of MOPITT CO and MERRA-2
29 vertical pressure velocity supported the transport of CO through the HC. Further, the results
30 revealed a distinct HC strength in two events (higher in 2006 compared to 2015) due to the

31 different El Niño conditions. Overall, the present findings can provide some insights into
32 understanding the regional transport of pollution over Southeast Asia and the role of climate
33 conditions on transport pathways.

34 **Keywords:** Indonesian fire pollution; Carbon monoxide; Lulin Atmospheric Background Station;
35 Hadley circulation

36 **1. Introduction**

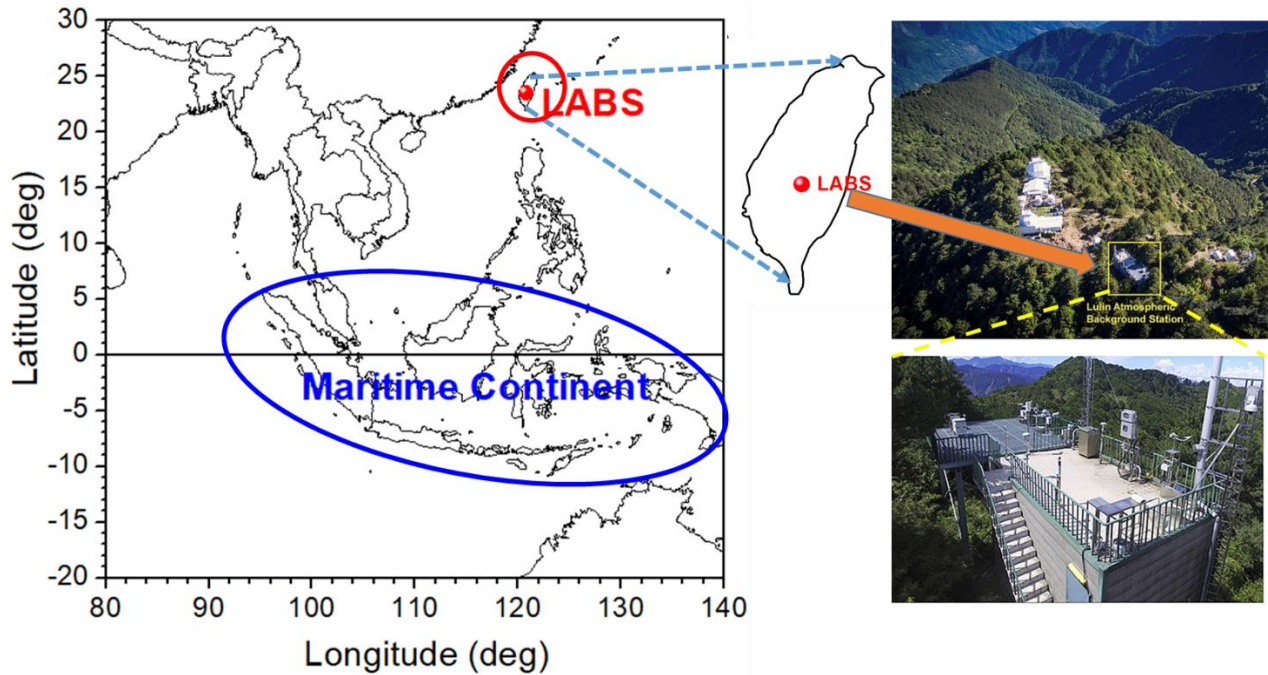
37 Fire activity over Southeast Asia (SEA), particularly over the Maritime Continent (MC,
38 including Indonesia), is a severe environmental problem that causes widespread regional pollution
39 in the lower troposphere and impacts atmospheric chemistry, air quality, and climate at regional
40 to global scales. Over the MC, fires occur predominately in the dry season (August to October)
41 and particularly during the periods of drought, often associated with the positive phase of El Niño-
42 Southern Oscillation (ENSO) events (Duncan et al., 2003a; van der Werf et al., 2008, 2017; Field
43 et al., 2009, 2016). A recent study has also highlighted the role of the Indian Ocean Dipole on MC
44 fire activity (Pan et al., 2018). For example, dry conditions associated with the positive IOD during
45 the 2015/16 and 2006/07 El Niño events led to increased fire activity over Indonesia and the wider
46 MC (van der Werf et al., 2008; Chandra et al., 2009; Nassar et al., 2009; Huijnen et al., 2016; Field
47 et al., 2016). Due to these intense fires, an enormous amount of carbon emissions was released
48 into the atmosphere in the form of carbon dioxide (CO₂), carbon monoxide (CO), and methane
49 (CH₄) (Huijnen et al., 2016; Field et al., 2016; Parker et al., 2016; Heymann et al., 2017). The
50 impact of these two Indonesian fire events on carbon emissions, tropospheric trace gases,
51 aerosol composition, and air quality has been extensively discussed in the literature (Chandra
52 et al., 2006; Logan et al., 2008; Chandra et al., 2009; Nassar et al., 2009; Huijnen et al., 2016;
53 Field et al., 2016; Heymann et al., 2017; Ravindra Babu et al., 2019). For example, the fire carbon
54 emissions during September-October 2015 over Maritime SEA were the largest since 1997
55 (Huijnen et al., 2016). By using Greenhouse gases Observing SATellite (GOSAT) data, Parker et
56 al. (2016) reported the strong enhancement of CO₂ and CH₄ over the Indonesian region.

57 CO is a significant emission from the combustion of fossil fuels and biomass (forest and
58 savanna fires, biofuel use, and waste burning) and is widely used as a tropospheric tracer for these
59 sources (Ou-Yang et al., 2014; Pani et al., 2019). Inter-annual variability of CO in the tropics and

60 sub-tropics is largely linked to year-by-year changes in biomass burning (BB) emissions.
61 Indonesian fires often emit large quantities of CO by incomplete combustion associated with the
62 occurrence of peat fire pollution. Although CO is not a direct greenhouse gas (GHG), it does have
63 a global warming potential due to its chemical reactions in the atmosphere. CO is also an ozone
64 (O_3) precursor in the troposphere, and indirectly increases radiative forcing ($0.23 \pm 0.05 \text{ W m}^{-2}$)
65 through the production of O_3 and CO_2 and depletion of hydroxyl radical, the primary chemical
66 reactant with CH_4 in the atmosphere (IPCC, 2013). The lifetime of CO in the free troposphere is
67 \sim two months, thus can be a tracer from polluted upwind regions to remote downwind areas
68 (Cooper et al., 2012). Some of the studies reported the influence of Indonesian fire activity and the
69 transport of CO from Indonesia to the Indian Ocean, Southern Pacific, and western Pacific Ocean
70 (Matsueda and Inoue, 1999; Pochanart and Akimoto, 2003; Nara et al., 2011; Matsueda et al.,
71 2002, 2019). However, the underlying transport mechanisms sending this fire pollution to
72 downwind northern hemisphere subtropical locations, particularly transport to high-altitude
73 background locations in the western north Pacific are still unclear.

74 Taiwan is located downwind of East Asia and Southeast Asia, which are major air pollutant
75 source regions. As a result, Lulin Atmospheric Background Station (LABS, $23.47^\circ\text{N } 120.87^\circ\text{E}$,
76 2862 m above sea level), was constructed in 2006 to study the transboundary transport of these air
77 pollutants and their impact on Taiwan. LABS is not affected by local sources, i.e., industrial and
78 traffic emissions, making it an ideal site for measuring long-range transport of air pollutants,
79 complementing the global network of the Global Atmospheric Watch (GAW) in the East Asia
80 region where no other high-altitude background station is available (Ou-Yang et al., 2014, 2022).
81 In the framework of Seven South-East Asian Studies (7-SEAS, Reid, et al., 2013; Lin et al., 2013;
82 Wang et al., 2015), several studies at LABS have reported on the long-range transport of northern
83 peninsular Southeast Asia (PSEA) BB pollutants to Taiwan through the low-level jet (LLJ) and
84 the related impacts on air quality and chemistry over Taiwan (Ou-Yang et al., 2012, 2014; Lin et
85 al., 2013; Chuang et al., 2016; Chi et al., 2016; Tsay et al., 2016; Hsiao et al., 2016; Lin et al.,
86 2017; Park et al., 2019; Pani et al., 2016, 2019; Huang et al., 2019; Huang et al., 2020; Ravindra
87 Babu et al., 2022a). However, to date, no studies have shown the potential influence of Indonesian
88 fire activities on LABS measurements and the BB pollution from Indonesian fires reaching LABS.
89 Surprisingly, the extensive fire events in 2006 and 2015 allowed us to track CO concentrations
90 from the Indonesian peat fires to LABS in Taiwan. By combining in-situ and satellite CO

91 measurements and large-scale circulation parameters from reanalysis products, we identified
92 plausible transport pathways from Indonesia to LABS.



93
94 **Figure 1.** Geographic location of the Maritime Continent and Lulin Atmospheric Background
95 Station (LABS, 23.47°N 120.87°E, 2862 m ASL), Taiwan.

96 **2. Site description, data, and methodology**

97 **2.1 Site description**

98 LABS is located on the summit of Mount Lulin and is shown in Figure 1, along with the location
99 of the Maritime Continent. Hiking is the only way to access LABS, taking about 30 minutes from
100 the nearest parking lot. There are no known point emission sources at the summit or in the
101 surrounding area with the exception of the occasional maintenance activity at the Lulin
102 Observatory. Because of the high altitude of LABS, measurements there are not affected by local
103 pollution from factories, traffic, and other domestic sources; rather, it is strategically located to
104 monitor long-range transported air pollutants from the Asian continent. More details about the
105 instruments and their specifications can be found in Sheu et al., 2009.

106

107

108 2.2 In-situ measurements

109 Details of the CO and various meteorological measurements at LABS employed in the
110 current study have been previously described in detail (Sheu et al., 2009; Ou-Yang et al., 2014;
111 Ravindra Babu et al., 2022b) and are thus only briefly described here. The long-term monthly
112 mean of various meteorological parameters such as temperature, relative humidity, wind speed,
113 and wind direction along with CO at LABS can be found in **Sup. Figure 1**. The overall mean
114 temperature (relative humidity) was about 10.5°C (~80%), with monthly mean temperatures
115 ranging between ~5 and 14°C. Local wind direction is mostly from the southwest and to a lesser
116 extent from the northeast. Long-term monthly mean in CO shows distinct seasonal patterns with a
117 springtime maximum and a summertime minimum at LABS. CO measurements were measured
118 by a nondispersive infrared (NDIR) analyzer (APMA-360, Horiba, Japan) at LABS. Hourly
119 averages of the 6-s data were analyzed in this study. The detection limit of the NDIR is ~20 ppb
120 (1σ) (Zellweger et al., 2009); more details about CO measured at LABS can be found in Ou-Yang
121 et. (2014). The magnitude of the CO concentration enhancement in 2006 and 2015 above the long-
122 term background was determined by comparing a 16-year average (2006-2021) of October CO
123 data at LABS. We obtained the percentage change in CO relative to the respective background
124 using Equation 1:

$$125 \quad \text{Relative change in percentage} = \left(\frac{x_i - \bar{x}}{\bar{x}} \right) \times 100 \quad (\text{Eq. 1})$$

126 where x_i represents the monthly mean of October in 2006 and 2015, and \bar{x} is the corresponding
127 monthly long-term mean calculated using the data from 2006 to 2021 (Ou-Yang et al., 2014).

128 2.3 Satellite measurements

129 CO observations from the Measurement of Pollution in the Troposphere (MOPITT, version
130 8) instrument were also utilized in this study (Worden et al., 2010; Deeter et al., 2019). MOPITT
131 is a multi-channel Thermal InfraRed (TIR) and Near InfraRed (NIR) instrument operating onboard
132 the sun-synchronous polar-orbiting NASA Terra satellite. V8 CO products, consisting of a CO
133 profile at ten pressure levels, have been validated; more details about the retrieval algorithm,
134 validation, and uncertainties of MOPITT CO can be found in Deeter et al. (2019). In addition to
135 the MOPITT measurements, we utilized CO from the Atmospheric Infrared Sounder (AIRS) on
136 the NASA Aqua satellite, which provides CO at different vertical levels twice daily and near-

137 global coverage. AIRS uses wavenumbers 2,183-2,200 cm^{-1} (4.58-4.5 μm) for retrieving CO
138 (McMillan et al., 2005). Version 8, level 3 CO product, available at $1^\circ \times 1^\circ$ resolution at various
139 pressure levels, was utilized in the present study. AIRS data were downloaded from the following
140 website https://disc.gsfc.nasa.gov/datasets/AIRS3STM_7.0 (AIRS project., 2019). AIRS
141 sensitivity to CO is broad and optimal in the mid-troposphere between approximately 300 and 600
142 hPa (Warner et al., 2007; Warner et al., 2013; AIRS project., 2019). CO retrievals have a bias of
143 6-10% between 900 hPa and 300 hPa with a root mean square error of 8-12 % (McMillan et al.,
144 2011).

145 Apart from MOPITT and AIRS CO data, we used Moderate Resolution Imaging
146 Spectroradiometer (MODIS) collection 6.1 daily active fire hot spot data from 2006–2021 over
147 Indonesia (Giglio et al., 2016).

148 **2.3 MERRA-2 Reanalysis products**

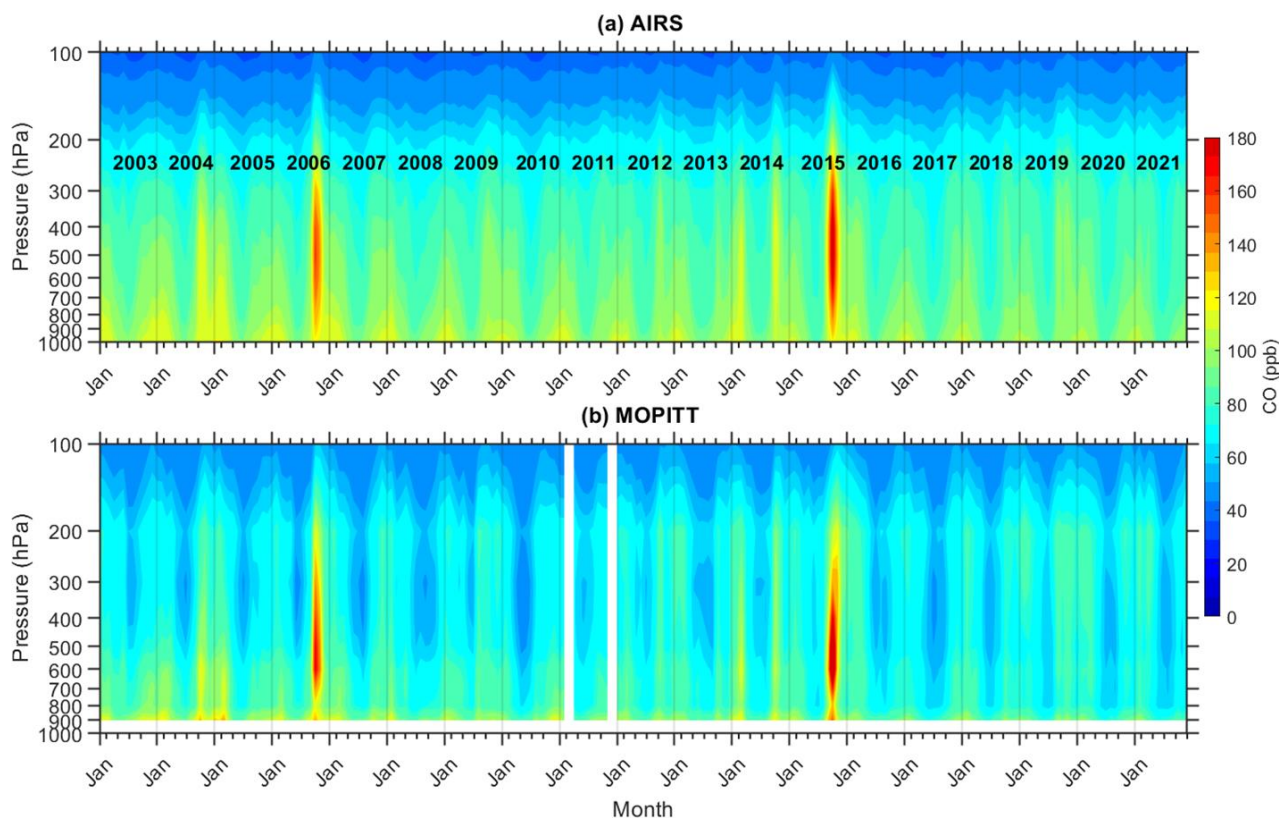
149 We also utilized monthly mean geopotential height (GPH), wind vectors (zonal and meridional
150 wind speed), and pressure vertical velocity from the Modern-Era Retrospective Analysis for
151 Research and Applications, version 2 (MERRA-2). MERRA-2 is the latest atmospheric reanalysis
152 data produced by the NASA Global Modeling and Assimilation Office (GMAO) (Gelaro et al.,
153 2017). The horizontal resolution of MERRA-2 reanalysis is $0.5^\circ \times 0.625^\circ$. MERRA-2 data are
154 available online through the NASA Goddard Earth Sciences Data Information Services Center
155 (GES DISC; <https://disc.gsfc.nasa.gov/>, last access: 11 September 2022).

156 **3. Results and Discussion**

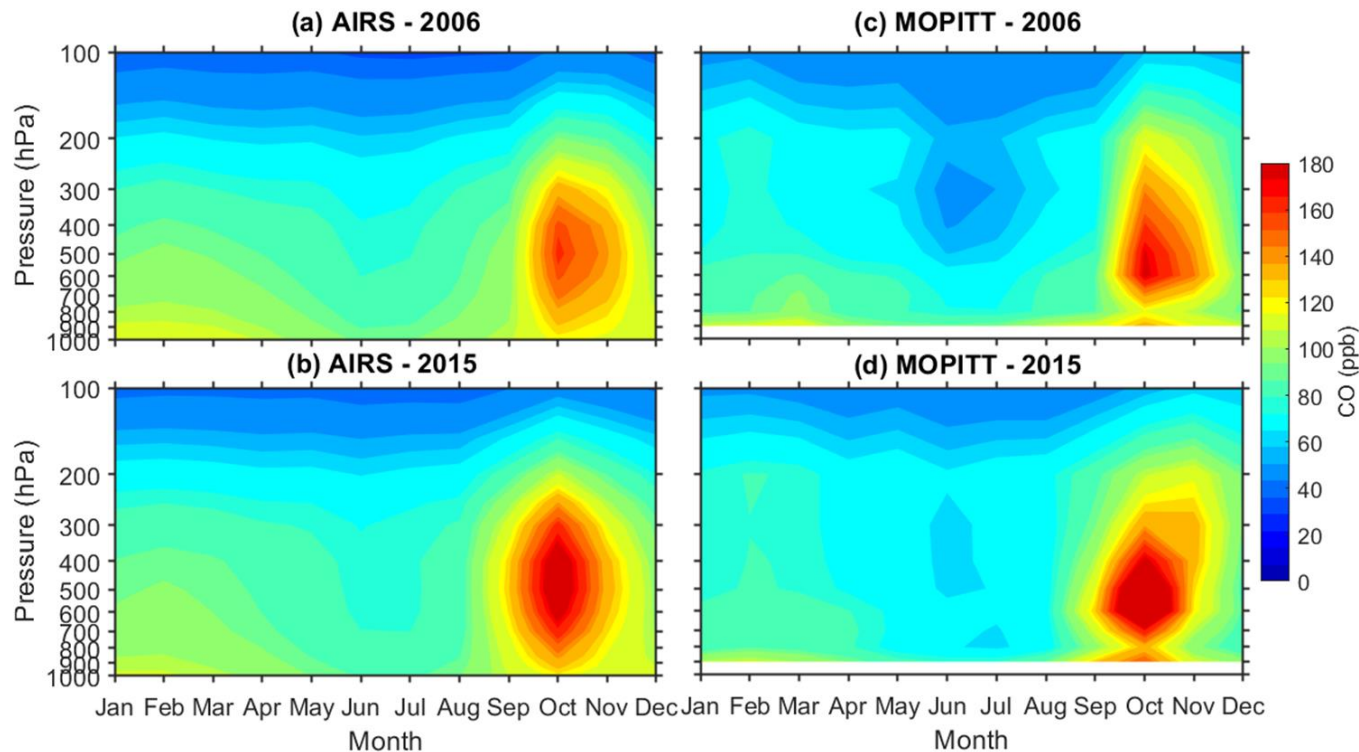
157 **3.1 Higher CO mixing ratios in October 2006 and 2015 over Maritime Continent and at** 158 **LABS**

159 **Figure 2** shows the height-time cross-section of monthly mean CO over the Maritime Continent
160 (MC) obtained from MOPITT and AIRS from 2003 to 2021. There is a significant inter-annual
161 variability in the CO time series in **Figure 2** as observed by both instruments. The maximum CO
162 mixing ratio for this time period was observed in the fall of 2006 and 2015; both were tied to El
163 Niño events (Field et al., 2016; Ravindra Babu et al., 2021; Ravindra Babu and Liou, 2021).
164 Several studies have reported on the impact of the intense fire activity in 2006 and 2015 and on
165 the release of significant carbon emissions and poor air quality over the wider Equatorial Asia

166 region (Logan et al., 2008; Chandra et al., 2009; Field et al., 2016; Huijnen et al., 2016; Ravindra
 167 Babu et al., 2019). Even though 2009 and 2014 were El Niño years, the CO over MC was not as
 168 high as observed in 2006 and 2015. The weaker and shorter duration of fire activities could largely
 169 explain the lower CO over the MC in 2009 and 2014 in contrast to those in 2006 and 2015.
 170 Furthermore, **Figure 3** shows the temporal variability of monthly mean CO from MOPITT and
 171 AIRS from January through December in both years 2006 and 2015, respectively. Both
 172 instruments show maximum CO enhancement in October compared to the remaining months in
 173 2006 and 2015. Overall, it is clear from **Figures 2** and **3** that in October 2006 and 2015, CO over
 174 the Maritime Continent in the entire troposphere increased dramatically due to increased CO
 175 emissions near the surface from extreme fire activity (**Fig. 4c**).



176
 177 **Figure 2.** Pressure-time cross-section of monthly mean carbon monoxide observed over the
 178 Maritime continent (average over 90E-140E, 10S-10N) during 2003-2021 obtained from (a) AIRS,
 179 and (b) MOPITT satellite measurements.



180

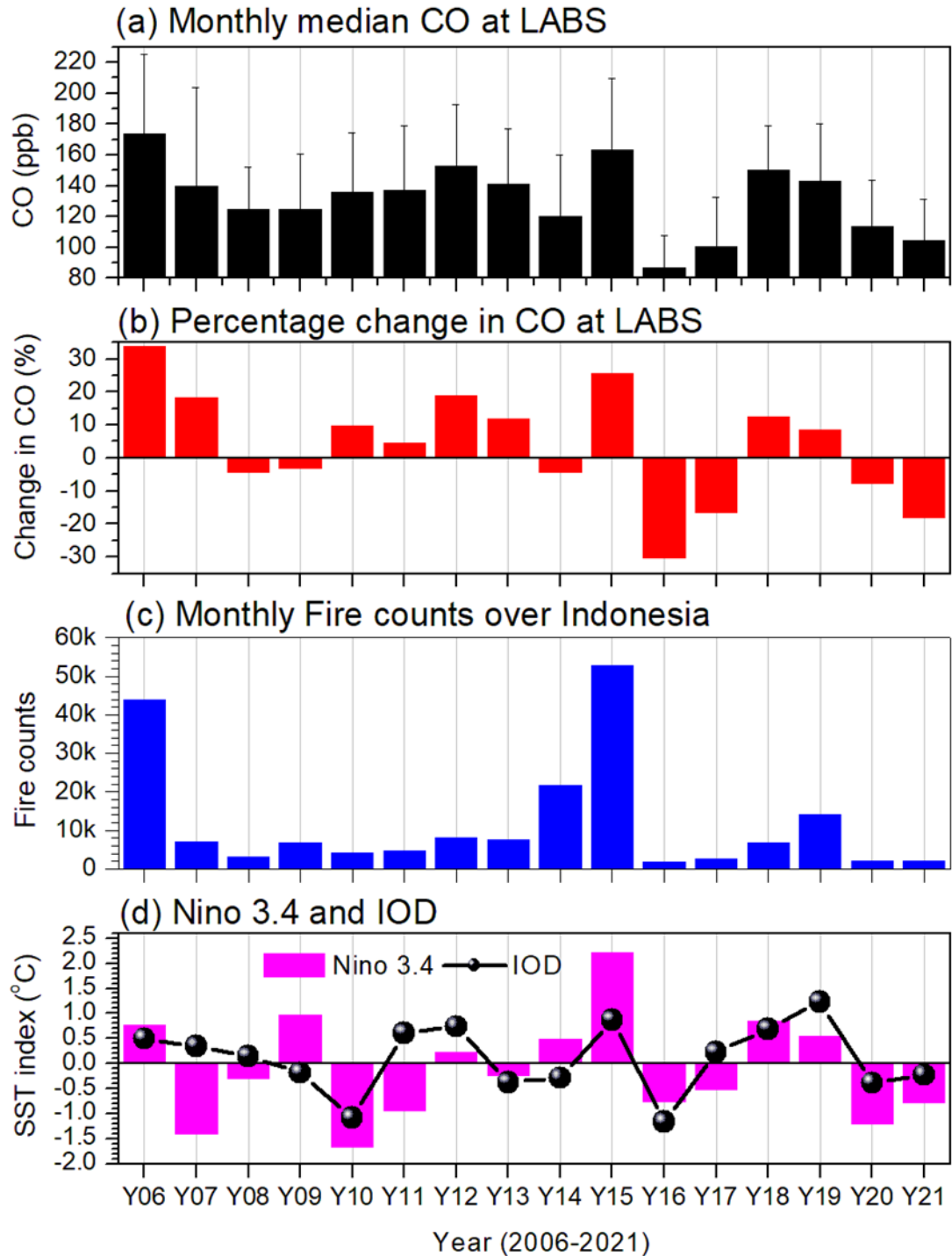
181 **Figure 3.** Pressure-time cross-section of monthly mean carbon monoxide observed over the
 182 Maritime continent (average over 90E-140E,10S-10N) in (a) 2006, (b) 2015 obtain from AIRS
 183 satellite measurements. Subplots (c) and (d) are the same as subplots (a) and (b) but for the
 184 MOPITT satellite measurements.

185 **Figure 4** summarizes the inter-annual variations of CO in October observed at LABS along
 186 with MODIS active fire counts over Indonesia and the observed Niño 3.4 and the IOD index
 187 values, which helped to motivate this study. The highest CO mixing ratios for this period were
 188 observed in 2006 and 2015, well over the long-term means of 132.1 ± 23.3 ppb when including all
 189 points and 126.8 ± 19.6 ppb when excluding 2006 and 2015. A significant enhancement of CO, over
 190 the latter mean calculation, of more than 47.2 ppb (37.2%) in 2006 and 36.7 ppb (28.9%) in 2015
 191 was observed, with the value in 2006 (2015) more significant than the $\pm 2\sigma$ ($\pm 1\sigma$) standard
 192 deviation of the long-term mean (**Table 1**). Higher CO mixing ratios in 2006 and 2015 at LABS
 193 was also evident from the MOPITT and AIRS satellite measurements obtained over a 1-degree
 194 radius around the LABS location (**Sup. Fig. 1**).

195 Unprecedented CO values in 2006 and 2015 at LABS could be due to the transport of CO
 196 from large-scale forest fires that were intense during the same period in the Indonesian region. It
 197 is clear from **Figure 4**, that the higher values of CO at LABS in 2006 and 2015 coincided with

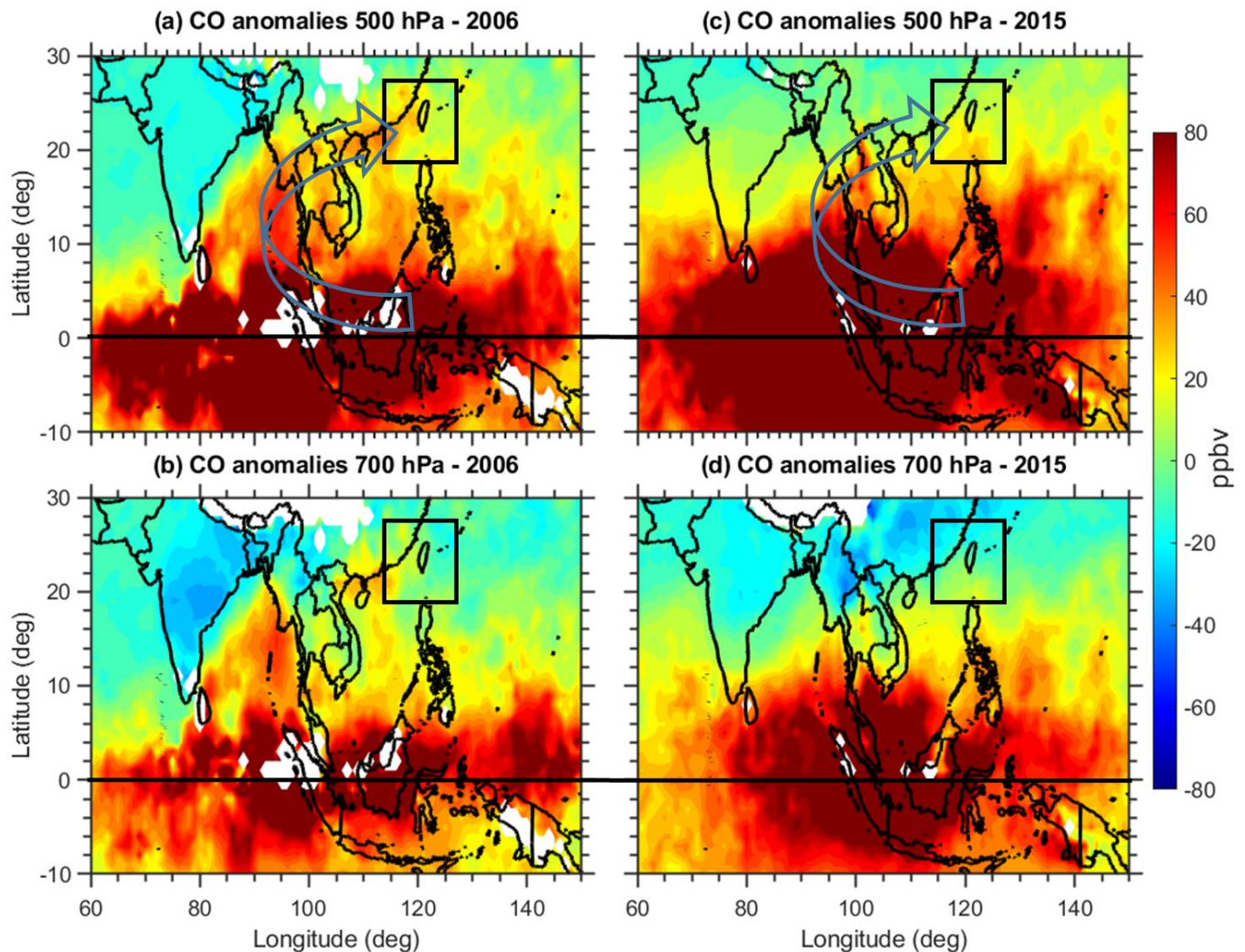
198 more intense fire activity over Indonesia along with warm phases of ENSO and IOD (**Fig. 4c and**
199 **4d**), which have been extensively studied due to the induced drought conditions in those years
200 (Field et al., 2016; Huijnen et al., 2016; Pan et al., 2018). Previous studies (e.g., Logan et al., 2008;
201 Zhang et al., 2011; Field et al., 2016; Pan et al., 2018) have demonstrated the direct relationship
202 between strong Indonesian fires and El Niño events. The enhanced CO values from the 2006 and
203 2015 events at LABS in the present study complement the findings of Matsueda and Inoue (1999)
204 in the case the of 1997 El Niño event and Nara et al. (2011) in the case of the 2006 El Niño event.
205 However, the impact on CO at LABS occurred significantly further north of the source region than
206 in either of the aforementioned studies. Based on aircraft measurements, Matsueda and Inoue
207 (1999) reported the enhancement of CO₂, CO, and CH₄ in the upper troposphere (at 9-12 km) over
208 the South China Sea (SCS) during October 1997 Indonesian fire event. However, this large CO
209 increase appeared only over the SCS west of Kalimantan and not in the subtropics between 10°N
210 and 26°N. Nara et al. (2011) reported a substantial increase in CO mixing ratios over the Western
211 Tropical Pacific Ocean (between 15°N and the Equator) by shipboard observations routinely
212 operated between Japan and Australia and New Zealand during October and November of 2006.
213 Similarly, Pochanart and Akimoto (2003) also reported the influence of the 1997 Indonesian fire
214 event on CO enhancement at the rural station Srinakarin (14°22'N, 99°07'E, 296 m above sea
215 level) in Thailand.

216 In addition, due to La Niña and the negative phase IOD, the fire activity in Indonesia during
217 2016 was much less intense than in 2006 and 2015 (**Fig. 4c and 4d**). Interestingly, CO at LABS
218 during 2016 exhibited the lowest October values in the entire data period, ~39.8 ppb (31.4%) lower
219 than the long-term October mean (2006-2021). It is well known that the major sources of CO at
220 LABS are BB from peninsular SEA in spring and industrial emissions from continental Asia in
221 winter (Ou-Yang et al., 2014; Pani et al., 2019; Ravindra Babu et al., 2022; Ou-Yang et al., 2022).
222 However, October is a transition month from the summer to winter at LABS, when air masses can
223 still arrive from the Pacific Ocean. Our analysis (**Fig. 4**) suggests that the extensive fires that
224 occurred during the 2006 and 2015 El Niño events over Indonesia may have yielded the
225 unprecedented CO mixing ratios at LABS in October of those years. Combined El Niño and IOD-
226 related changes in the large-scale dynamics and circulations may have promoted CO emissions
227 from Indonesian fires to transport to LABS.



228

229 **Figure 4.** Inter-annual variations in October of the (a) monthly median of CO, (b) percentage
 230 change in CO from the long-term mean at LABS, (c) MODIS (Moderate Resolution Imaging
 231 Spectroradiometer) total active fire counts (only fires tagged with >30 % confidence) over
 232 Indonesia, (d) sea surface temperature index for Niño 3.4 (magenta) and Indian ocean dipole
 233 (black) during 2006 to 2021.



234

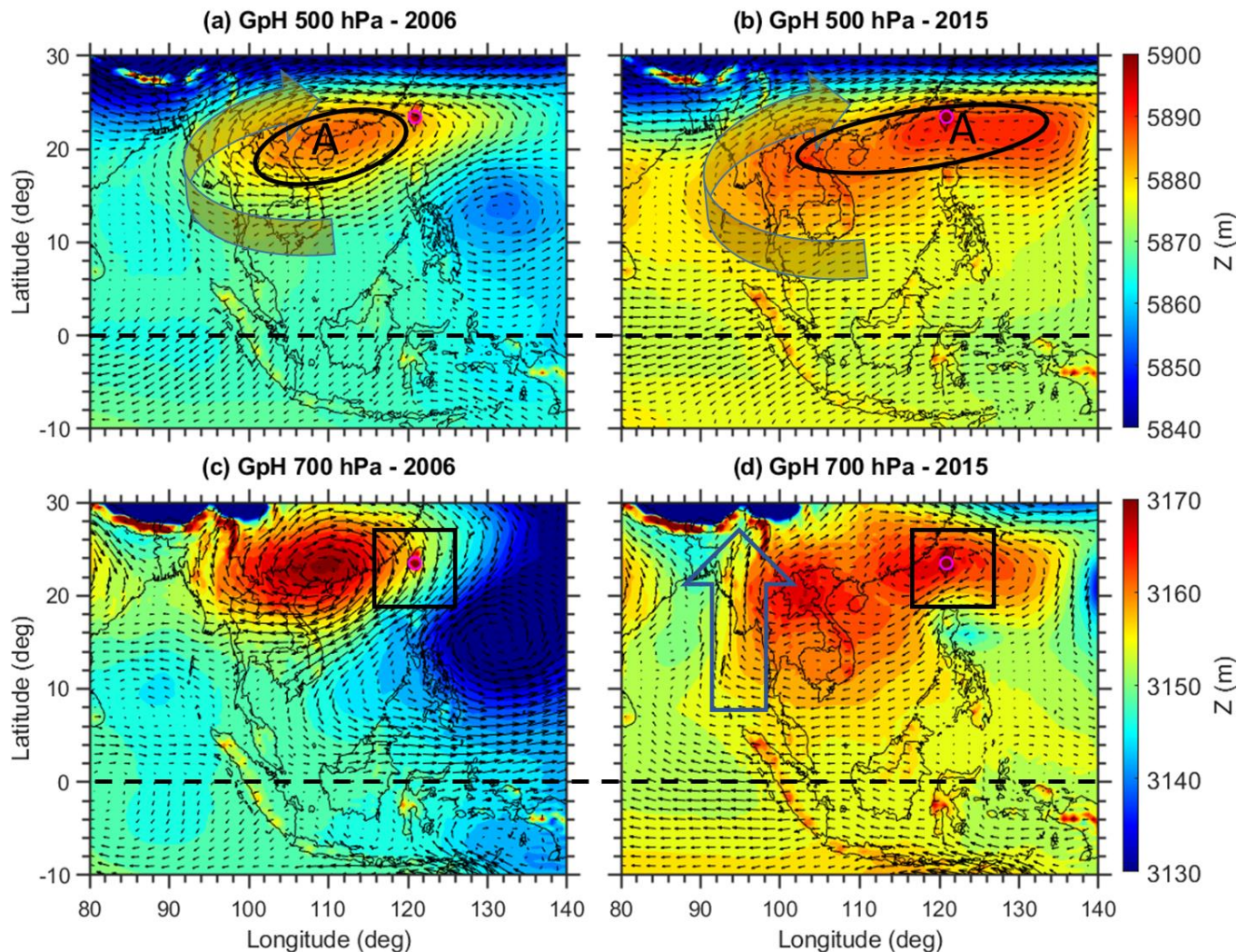
235 **Figure 5.** Monthly mean CO anomalies obtained from MOPITT satellite observations (a) at 500
 236 hPa and (b) at 700 hPa during October 2006. Subplots (c) and (d) are the same as subplots (a) and
 237 (b) but for October 2015, respectively. The anomalies are obtained by subtracting the 2006 and
 238 2015 data from the long-term mean of MOPITT CO data from 2001 to 2021.

239 To confirm the impact of Indonesian fire pollution on LABS CO, we further checked the
 240 spatial distribution of CO in 2006 and 2015 from the MOPITT satellite CO observations. An inter-
 241 comparison between October monthly mean CO at LABS (2006-2021) and MOPITT and AIRS
 242 CO data at 700 hPa within the 1-degree radius around the LABS location yielded correlation
 243 coefficients of 0.88 and 0.78 ($p < 0.01$), respectively (**Sup. Fig. 2**). We then used the MOPITT
 244 satellite data to track the spatial and vertical CO changes in October 2006 and 2015; first, we
 245 examined the distribution of the CO anomalies at free tropospheric heights in those years. **Figure**
 246 **5** shows these anomalies compared to the long-term mean (2001-2021) at 700 hPa and 500 hPa,
 247 revealing extensive enhancements of CO mixing ratios over most of equatorial Asia in 2006 and

248 2015. **Figure 5** indicates that CO from the Indonesian fires affected both the Indian Ocean to the
249 west and South Pacific and the northern Pacific to the east. Furthermore, these outflows of CO
250 split northwestward into the Bay of Bengal and northeastward into the western North Pacific. It is
251 also worth noting that the anomalies were significantly higher at 500 hPa than at 700 hPa. Elevated
252 CO is visible in the Taiwan region at 700 hPa and 500 hPa in both years. This further provides a
253 clear signature of the impact of Indonesian fire activity on enhanced CO in 2006 and 2015 at
254 LABS. Overall, from **Figure 5**, MOPITT CO data shows the Indonesia fires transported CO
255 vertically and horizontally in all directions. We further investigated the associated dynamics and
256 large-scale circulations supporting the transport of Indonesian pollution to LABS.

257 **3.2 Role of large-scale dynamics and atmospheric circulations**

258 Large-scale dynamics and circulations can play a crucial role in transporting Indonesian
259 pollution to long-distance downwind regions (Bowman, 2006; Nara et al., 2011; Matsueda et al.,
260 2019). To understand the plausible mechanisms behind the transport of Indonesian fire pollution
261 to LABS, we further examined the MERRA-2 reanalysis of geopotential height (GpH) and wind
262 distribution in 2006 and 2015. The spatial distribution of GpH at two pressure levels (700 and 500
263 hPa) in both events is shown in **Figure 6**. The GpH and wind vectors in the two event years
264 exhibited quite different patterns in relation to a high-pressure system over the northern parts of
265 the SCS. A high-pressure anti-cyclonic circulation center extended from the Indo-China Peninsula
266 to the SCS in October 2006 with LABS located precisely on the eastern edge of the anticyclone.
267 In 2015, the anticyclone extended from the Indo-China Peninsula to the western North Pacific
268 region and over Taiwan.



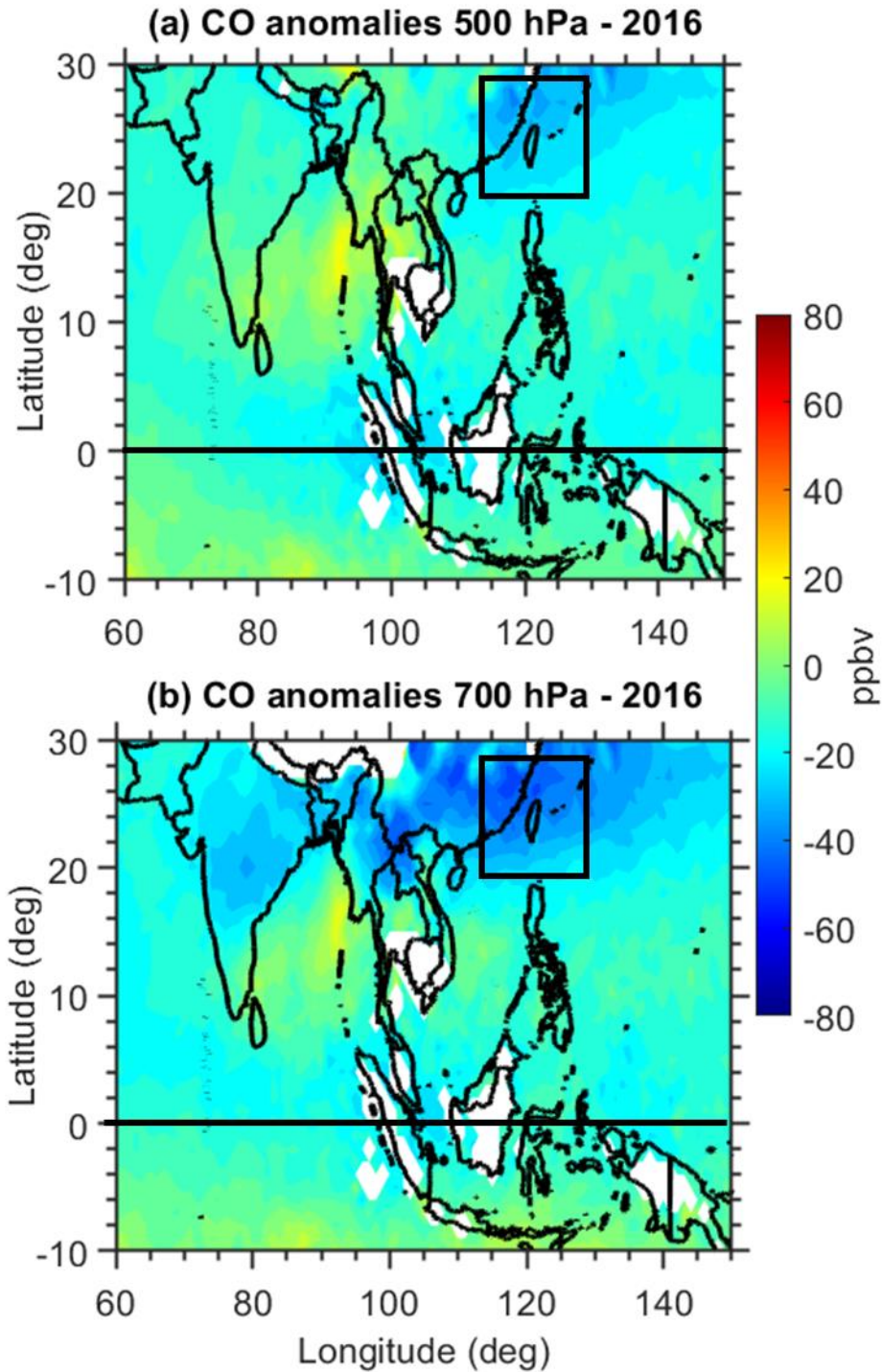
269

270 **Figure 6.** Monthly mean Geopotential height (GpH) obtained from MERRA-2 reanalysis (a) at
 271 500 hPa and (b) at 700 hPa during October 2006. Subplots (c) and (d) are the same as subplots (a)
 272 and (b) but for October 2015.

273 During both event years, strong southerlies at 500 hPa were evident due to the high-
 274 pressure anticyclone system in the northern SCS. It is assumed that the northern edge of the
 275 Indonesian fire pollution plume can be carried out by the southerlies and around the western edge
 276 of the high-pressure anti-cyclone over SCS. An apparent merging of the southerlies from the
 277 equator with the subtropical westerlies in the northern PSEA region subsequently led to the
 278 transport of CO to downwind LABS. Overall, in both events, there was a significant anticyclone
 279 over the SCS. El Niño and the positive IOD-induced high-pressure anticyclone over SCS
 280 strengthen the southerlies from the equator, consequently bringing higher amounts of CO to LABS.
 281 We further investigated the vertical pressure velocity (ω) behavior in both events (**Sup. Fig**

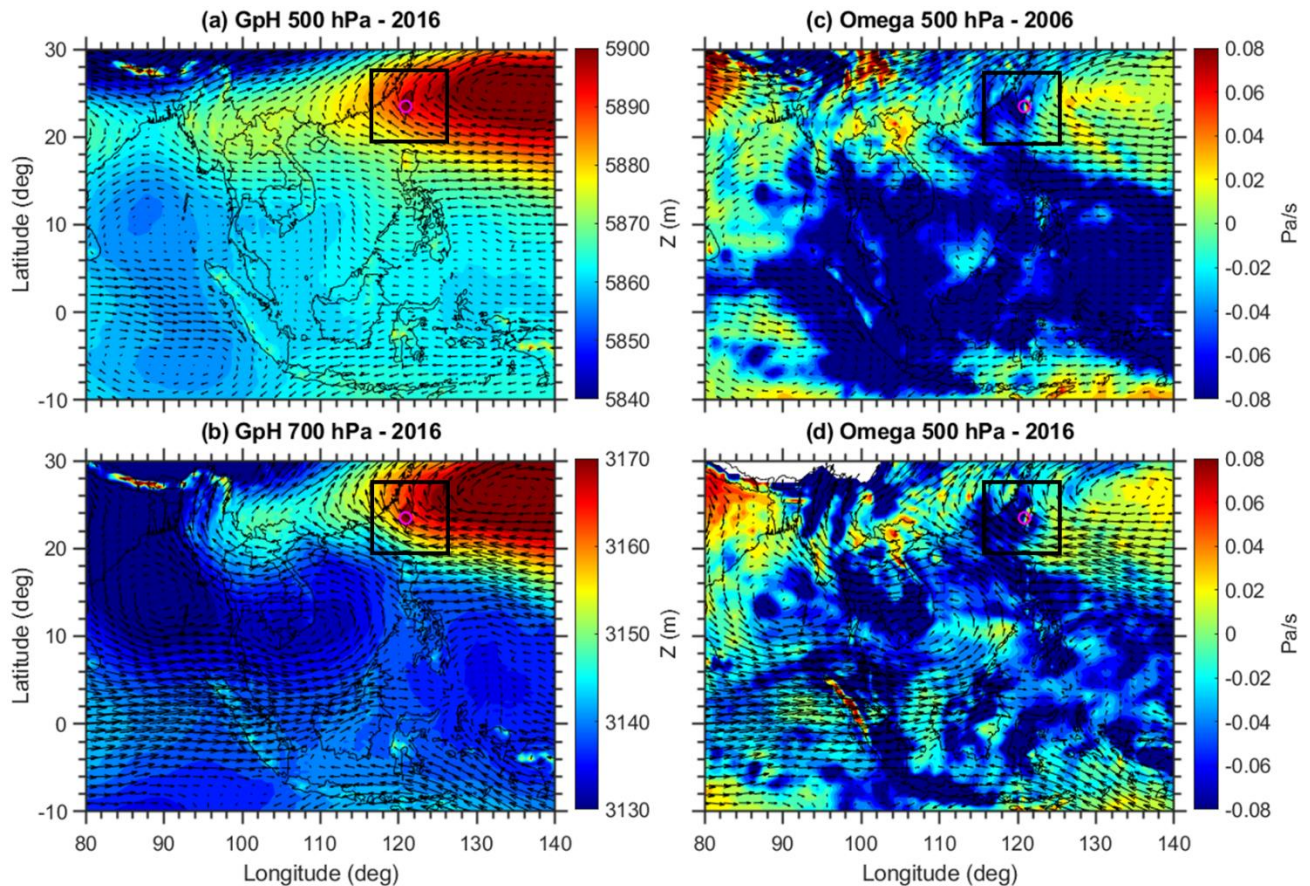
282 **3**), where negative (positive) values represent upward (downward) winds. Significant upward wind
283 in both events was evident over equatorial MC, while vertical pressure velocity over Taiwan and
284 surrounding regions at both pressure levels were mostly downwards in 2006 and 2015. The
285 presence of a downwind will provide downward transport of any pollutant presence in the upper
286 troposphere over that region. Also, the downward wind was relatively higher in 2006 compared to
287 2015. The center of the downward wind was shifted eastwards in the western North Pacific in
288 2015. The distinct behavior of vertical pressure velocity around LABS during these two events
289 might be due to the associated climate conditions in the two periods; more discussion will be
290 provided in section 3.4.

291 We further showed CO deviations at both pressure levels in October 2016 when there was
292 very low fire activity in Indonesia (**Fig. 7**). Interestingly, there was a significant lowering of CO
293 over the Taiwan region in 2016, which agrees with the observed low CO values from the in-situ
294 measurements at LABS (**Fig. 4b**). Also in agreement, 2016 was a La Niña and negative IOD year
295 and fire activity was much weaker (**Fig. 4c** and **4d**). During the La Niña years, large-scale
296 dynamical processes are greatly reversed with respect to El Niño years. We further analyzed the
297 GpH and wind circulation patterns in 2016 (**Fig. 8**). A significant high-pressure system (western
298 North Pacific subtropical High) was present over the western North Pacific region in 2016, which
299 was shifted considerably further eastward compared to the SCS in 2006 and 2015. The wind
300 vectors also highlighted the transport of a clean marine air mass from the Pacific Ocean to LABS
301 in 2016. Interestingly, the vertical pressure velocity exhibited a pronounced upward wind over
302 Taiwan in 2016, in contrast to the downward wind in 2006 and 2015. This indicates that dominant
303 clean marine air reached LABS in 2016 resulting in the lowest CO mixing ratio in the entire dataset
304 at LABS.



305

306 **Figure 7.** Monthly mean CO deviations from the long-term mean (2001-2021) were obtained
 307 from MOPITT satellite observations (a) at 500 hPa and (b) at 700 hPa during October 2016.



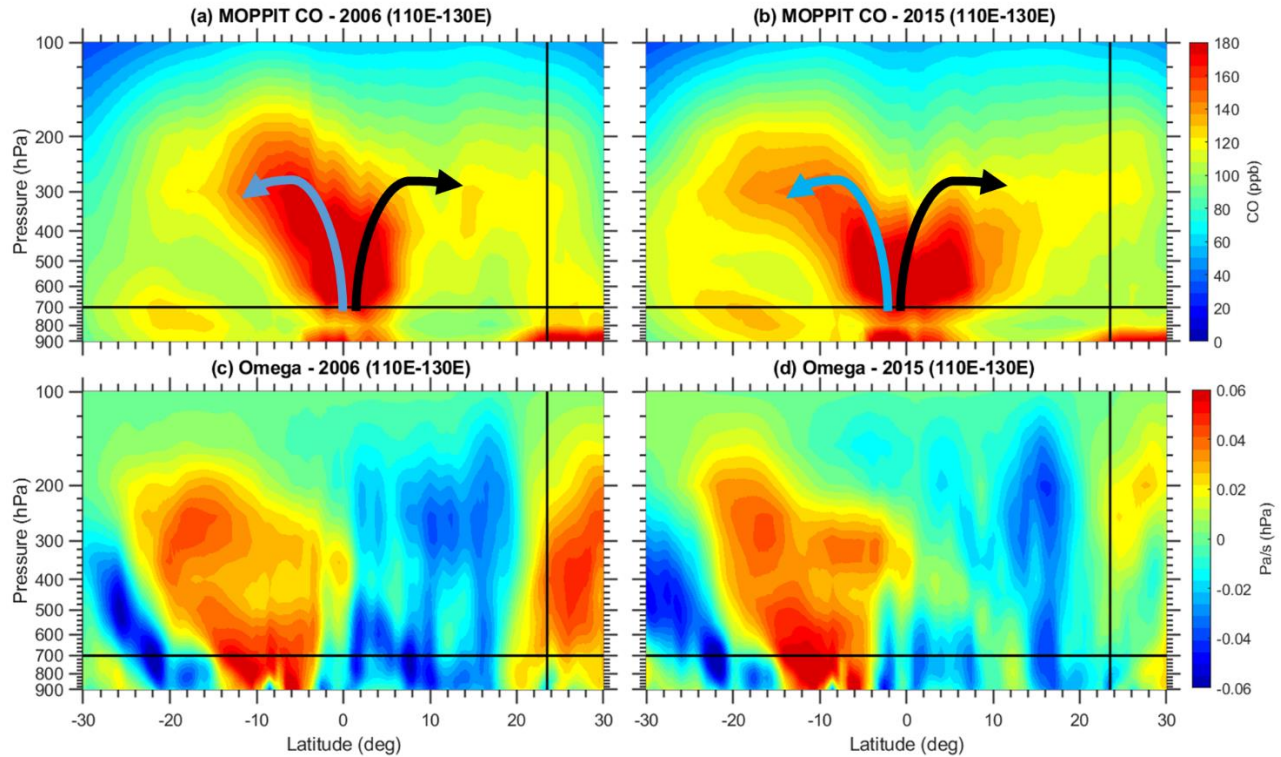
308

309 **Figure 8.** Monthly mean Geopotential height (GpH) obtained from MERRA-2 reanalysis (a) at
 310 500 hPa, and (b) at 700 hPa during October 2016. The subplots (c) and (d) are the same as subplots
 311 (a) and (b) but for the observed vertical pressure velocity (Omega).

312 3.4 Role of Hadley circulation

313 The Hadley circulation (HC) is a crucial component of the climate system, which is
 314 characterized by a thermally driven large-scale meridional circulation (Hadley, 1735). This
 315 circulation links the troposphere and stratosphere and the tropics and extra-tropics, through
 316 horizontal and vertical motions, transporting moisture, heat, and momentum to regulate Earth's
 317 energy budget. As the CO sources (Indonesia) in this study were close to the equator, it is expected
 318 that air tends to rise more or less directly over the CO sources. **Figure 9** shows the vertical-
 319 meridional cross-section of CO and vertical pressure velocity in separate panels averaged between
 320 110°–130°E in October 2006 and 2015. The black-colored vertical line in all the panels in **Figure**
 321 **9** shows the location of LABS and the horizontal line represents the 700 hPa. The vertical cross-
 322 section of CO highlights the uplifting of CO into the upper troposphere over the equator, followed
 323 by southward and northward movement in both 2006 and 2015 (**Fig. 9a** and **9b**). A clear transport

324 of CO from the source region to the sub-tropics via meridional transport was evident in both events.
325 It is noted that the higher CO observed between 20–30°N latitude below ~700 hPa is related to
326 anthropogenic emissions and not due to the Indonesian fires. To confirm the lofted CO from
327 Indonesia really descended in the subtropics due to the Hadley circulation, we looked into the
328 vertical cross-section of vertical pressure velocity in both events. From **Figure 9**, it is suggested
329 that large amounts of CO from Indonesia were transferred into the free troposphere by the strong
330 upward air motion in this region. Similarly, there was a pronounced descending motion (positive
331 values of vertical pressure velocity) during October 2006 (**Fig. 9c**) in the northern hemisphere
332 subtropics around 20–30°N latitude, which corresponds well with the location of LABS. However,
333 in October 2015, the descending motion was not significant compared to 2006. This may be due
334 to the different El Niño conditions in 2006 and 2015. While IOD conditions were indeed similar
335 between 2006 and 2015 (**Fig. 4d**), the higher descending motions in 2006 can be explained in part
336 by the moderate El Niño conditions during that year. A well-developed El Niño condition was
337 already established in 2015 compared to 2006. In October 2006, the observed Niño 3.4 value was
338 around 0.7 whereas in 2015 it was around 2.21. These values indicate that the El Niño conditions
339 were already well established in October 2015 whereas, in 2006, the conditions were not developed
340 as El Niño. It is reported that in El Niño conditions, the western Pacific HC is observed to be
341 weakened whereas the eastern Pacific HC is strengthened (Wang, 2004). This is supported by the
342 observed lesser descending motions in 2015 from the present study. These differences in the
343 descending motions likely influenced the greater CO enhancement in 2006 compared to 2015 at
344 LABS (**Fig. 4b** and **Table 1**). Overall, it is clearly illustrated from the MOPITT CO vertical cross-
345 section and the MERRA-2 vertical pressure velocity that the CO emitted from the Indonesian fire
346 was transported vertically through the Hadley circulation to the LABS location.

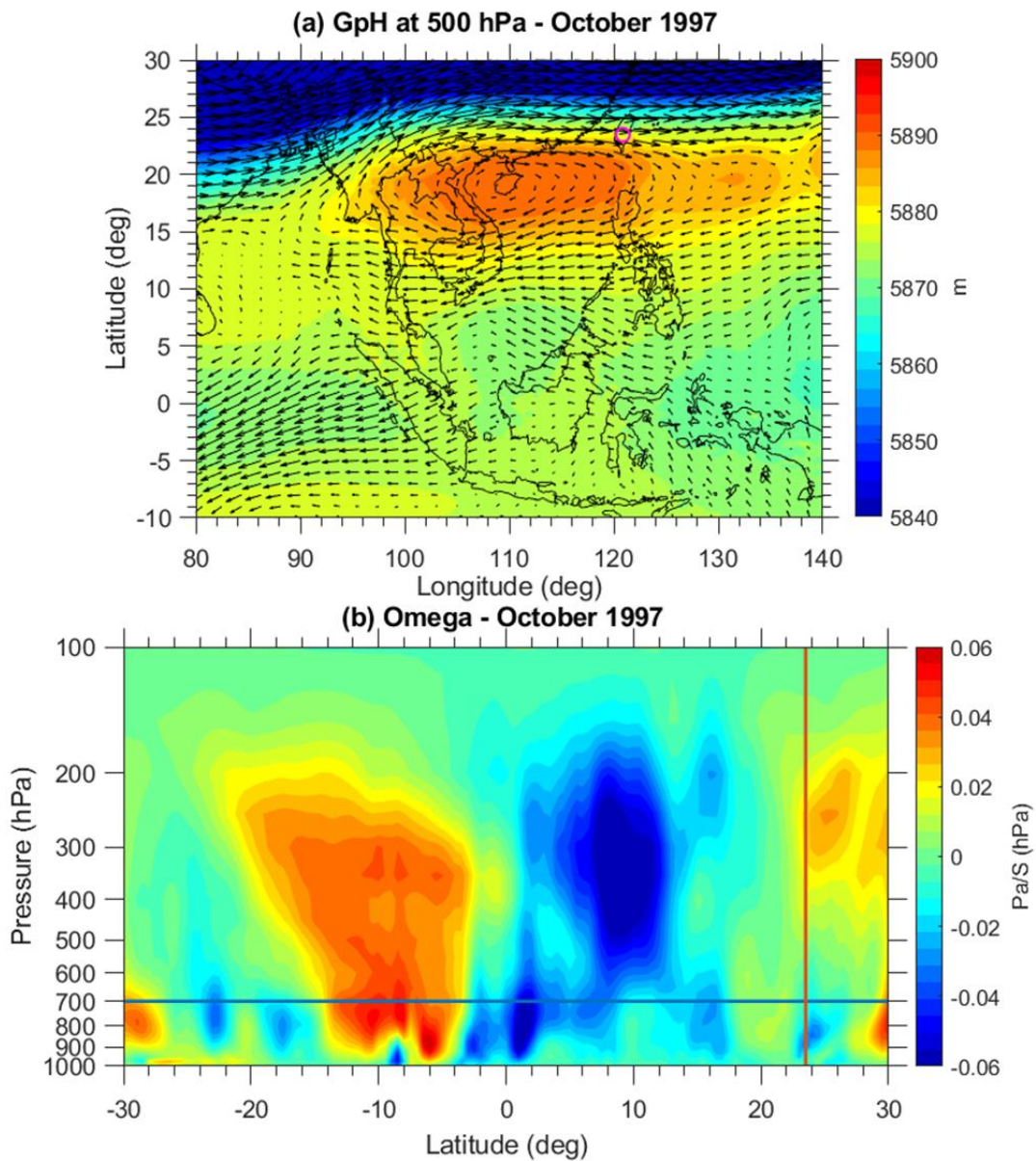


347

348 **Figure 9.** Pressure–latitude cross-section of MOPITT CO averaged along 110°–130°E (a) for
 349 October 2006 and (b) for October 2015. Subplots (c) and (d) are the same as subplots (a) and (b)
 350 but for the MERRA-2 reanalysis vertical pressure velocity. Positive (negative) values represent
 351 the downward (upward) wind.

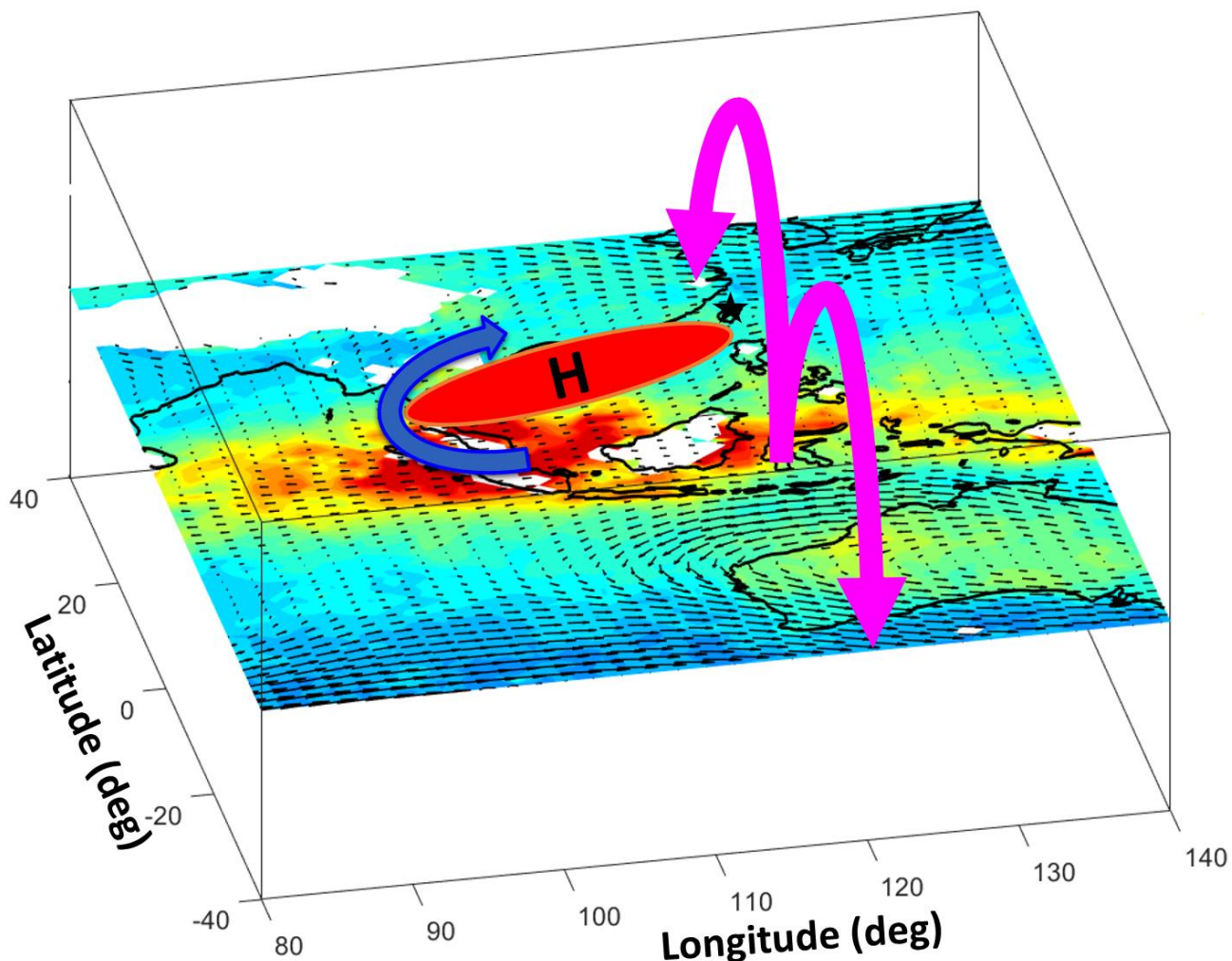
352 One of the worst fire events in Indonesia’s history occurred in October 1997 and was
 353 associated with an El Niño event and a positive IOD (Duncan et al., 2003a). In order to see any
 354 similarities between 1997 and 2006 and 2015, particularly in large-scale circulations, we further
 355 checked the MERRA-2 GpH and wind circulation pattern in October 1997. To note, none of the
 356 satellite measurements of CO (either AIRS or MOPITT) are available during the 1997 event, and
 357 measurements at LABS didn’t start until 2006. Hence, we only cross-checked the large-scale
 358 circulations that are observed in October 1997, respectively. **Figure 10a** shows the spatial
 359 distribution of GpH observed at 500 hPa and **Figure 10b** shows the vertical-meridional cross-
 360 section of vertical pressure velocity averaged along 110°–130°E in October 1997. Interestingly,
 361 we noticed a significant high-pressure anti-cyclonic circulation over northern parts of the SCS in
 362 October 1997 as observed in 2006 and 2015. Also evident is the merging of the southerlies from
 363 the MC with the subtropical westerlies in the northern PSEA region. Similarly, the vertical
 364 pressure velocity also shows the upward wind over the MC and the downward wind over the
 365 northern hemisphere subtropics around 20–30°N latitude. From Sup. Figure 4b, it is very clear that

366 a significant descending wind was evident around the LABS location in 1997 similar to 2006 and
367 2015. Overall, it is very clear from the present results that it is possible to transport pollution from
368 Indonesia to sub-tropical East Asia during extreme and higher-duration fire events like 1997, 2006,
369 and 2015.



370
371 **Figure 10.** MERRA-2 reanalysis (a) Monthly mean Geopotential height (GpH) at 500 hPa, and
372 (b) pressure-latitude cross-section of vertical pressure velocity observed on October 1997.

373



374

375 **Figure 11.** Schematic diagram of CO transport from Indonesian fires to subtropical East Asian
 376 region. The horizontal transport of CO due to the high-pressure anticyclone is denoted by the blue-
 377 colored arrow. H denotes a high-pressure anticyclone over northern parts of the South China Sea.
 378 Magenta-colored arrows indicate the transport of CO through the local Hadley circulation (over
 379 110°–130°E). Black-colored star symbol represents the LABS location.

380 The major transport pathways of CO from Indonesia to subtropical East Asia are illustrated
 381 in a schematic diagram (**Fig. 11**). Illustrated mechanisms include horizontal transport in the free
 382 troposphere due to El Niño and positive IOD-induced high-pressure anticyclone circulation, and
 383 vertical transport through the Hadley circulation. The southerlies on the southwest flank of the
 384 anticyclone merged with the subtropical westerlies over PSEA and then transported polluted air to
 385 LABS. Apart from this horizontal transport, CO was transported through the Hadley circulation to
 386 LABS in both events. However, there was a distinctly different Hadley Circulation strength in

387 2006 compared to 2015 due to the different El Niño conditions. These two events were strongly
388 associated with positive IOD, but in 2006, the El Niño conditions were not well-developed,
389 whereas in 2015 well-developed El Niño conditions were evident. These El Niño conditions
390 further suppressed the HC over the western Pacific in 2015 compared to 2006. This suggested the
391 importance of the background climate conditions (ENSO and IOD) on the pollutant transport
392 process.

393 **4. Summary and Conclusions**

394 Due to the combined impact of positive phase IOD and El Niño-induced drought
395 conditions in 2006 and 2015, Indonesia experienced extreme fire activity. MODIS active fire
396 counts showed the largest fires in October 2006 and 2015 compared to the other years in the 16-
397 year period in Indonesia. These record fires reflected two of the largest carbon emissions in the
398 Indonesian region since 1997. Lulin Atmospheric Background Station (LABS, 23.47°N 120.87°E,
399 2862 m ASL) is the only high-altitude background station located in the western North Pacific
400 region, and is optimally located to study some of these transport processes, including long-range
401 transport of pollution in the free troposphere and stratospheric intrusions. Interestingly, during
402 these two events (October 2006 and 2015), we noticed an abnormal enhancement of CO compared
403 to other years at LABS from the in-situ measurements. In the present study, for the first time, the
404 impact of Indonesia fire pollution on CO measurements at LABS and the plausible transport
405 pathways for the transport of CO from Indonesia to sub-tropical East Asia were investigated. The
406 main findings are summarized below:

- 407 1. Compared to 16-year (2006-2021) means, a substantial increase in CO mixing ratios of
408 about ~47.2 ppb (37.2%) in October 2006 and ~36.7 ppb (28.9%) in October 2015 was
409 observed at LABS.
- 410 2. By comparing the CO and atmospheric large-scale circulation data, we found two plausible
411 transport pathways of CO from Indonesia to LABS. i.e. horizontal transport in the free
412 troposphere and vertically through the Hadley Circulation.
- 413 3. El Niño and positive IOD-induced high-pressure anticyclone circulation over northern
414 parts of the South China Sea play an important role in the horizontal transport of CO.

415 4. Distinct strength of the Hadley circulation over the western Pacific was observed in
416 October 2006 (stronger) and 2015 (weaker). Well-developed El Niño conditions in
417 October 2015 suppressed the strength of the Hadley Circulation over the western Pacific.

418 A changing warmer climate can influence carbon emissions and alter the transport pathways, hence
419 impacting the various scales of air pollution and climate. Changes in the background climate will
420 inevitably impact meteorological transport processes and the concentrations of pollutants arriving
421 at downwind regions. Overall, the present results further provide knowledge to the atmospheric
422 chemistry community about the different transport pathways of pollutants and the role of climate
423 conditions.

424 **Data availability**

425 The CO data at LABS can be assessed at http://lulin.tw/index_en.htm. The AIRS and MOPITT
426 CO data can be downloaded from the following websites
427 https://disc.gsfc.nasa.gov/datasets/AIRS3STM_7.0 (AIRS project., 2019) and
428 <https://asdc.larc.nasa.gov/project/MOPITT>. MERRA-2 data are available online through the
429 NASA Goddard Earth Sciences Data Information Services Center (GES DISC;
430 <https://disc.gsfc.nasa.gov>, last access: 30 May 2022). Nino 3.4 Index and IOD data can be
431 downloaded through the following websites https://psl.noaa.gov/gcos_wgsp/Timeseries/Niño34/.
432 https://psl.noaa.gov/gcos_wgsp/Timeseries/DMI/. The MODIS fire products can be downloaded
433 from the following website https://firms.modaps.eosdis.nasa.gov/active_fire/.

434 **Author contributions**

435 **Saginela Ravindra Babu:** Conceptualization, Data curation, Formal analysis, Investigation,
436 Software, Validation, Visualization, Writing – original draft preparation, Writing – review and
437 editing; **Chang-Feng Ou-Yang:** Data curation, Software, Validation, Visualization; **Stephen M.**
438 **Griffith;** Writing – review and editing; **Shantanu Kumar Pani:** Data curation and Visualization;
439 **Steven S. Kong:** Data curation and Visualization; **Neng-Huei Lin:** Conceptualization,
440 Investigation, Funding Acquisition, Supervision, Resources, Writing – review and editing.

441 **Competing Interest**

442 The authors declare that they have no conflict of interest.

443 **Acknowledgments**

444 The work is primarily supported by the Ministry of Science and Technology, Taiwan under the
445 grants of MOST 110-2811-M-008-562 and MOST 109-2811-M-008-553. Authors thanks to
446 Taiwan Environmental Protection Administration (TEPA) for supporting the air pollutants
447 monitoring at LABS. The authors thank NASA and NOAA for providing MOPITT, MODIS, and
448 AIRS satellite data. We thank NASA's Global Monitoring and Assimilation Office (GMAO) for
449 providing the Modern-Era Retrospective analysis for Research and Applications, Version 2
450 (MERRA-2) data. We also thank NOAA ESRL Physical Sciences Laboratory for providing Indian
451 Ocean Dipole and Niño 3.4 index values through the following websites
452 https://psl.noaa.gov/gcos_wgsp/Timeseries/DMI/
453 https://psl.noaa.gov/gcos_wgsp/Timeseries/Niño34/.

454 **5. References**

- 455 AIRS project (2019), Aqua/AIRS L3 Monthly Standard Physical Retrieval (AIRS-only) 1-degree
456 x 1 degree V7.0, Greenbelt, MD, USA, Goddard Earth Sciences Data and Information Services
457 Center (GES DISC), Accessed: (11 September 2022), 10.5067/UBENJB9D3T2H.
- 458 Bowman, K. P. and Cohen, P. J.: Interhemispheric exchange by seasonal modulation of the Hadley
459 circulation, *J. Atmos. Sci.*, 54, 2045–2059, [https://doi.org/10.1175/1520-
460 0469\(1997\)054%3C2045:IEBSMO%3E2.0.CO;2](https://doi.org/10.1175/1520-0469(1997)054%3C2045:IEBSMO%3E2.0.CO;2), 1997.
- 461 Bowman, K. P.: Transport of carbon monoxide from the tropics to the extratropics, *J. Geophys.*
462 *Res.-Atmos.*, 111, <https://doi.org/10.1029/2005JD006137>, 2006.
- 463 Chandra, S., Ziemke, J. R., Duncan, B. N., Diehl, T. L., Livesey, N. J. and Froidevaux, L.: Effects
464 of the 2006 El Niño on tropospheric ozone and carbon monoxide: implications for dynamics
465 and biomass burning, *Atmos. Chem. Phys.*, 9, 4239–4249, [https://doi.org/10.5194/acp-9-4239-
466 2009](https://doi.org/10.5194/acp-9-4239-2009), 2009.
- 467 Chandra, S., Ziemke, J. R., Schoeberl, M. R., Froidevaux, L., Read, W. G., Levelt, P.F. and
468 Bhartia, P. K.: Effects of the 2004 El Nino on tropospheric ozone and water vapor,
469 *Geophys.Res. Lett.*, 34, L06802, <https://doi.org/10.1029/2006GL028779>, 2007.

470 Chi, K.H., Hung, N.T., Lin, C.Y., Wang, S.H., Ou-Yang, C.F., Lee, C.T. and Lin, N.H.: Evaluation
471 of Atmospheric PCDD/Fs at Two High-Altitude Stations in Vietnam and Taiwan during
472 Southeast Asia Biomass Burning. *Aerosol Air Qual. Res.* 16: 2706-2715.
473 <https://doi.org/10.4209/aaqr.2015.11.0653>, 2016.

474 Chuang, M. T., Fu, J. S., Lee, C. Te, Lin, N. H., Gao, Y., Wang, S. H., Sheu, G. R., Hsiao, T. C.,
475 Wang, J. L., Yen, M. C., Lin, T. H. and Thongboonchoo, N.: The simulation of long-range
476 transport of biomass burning plume and short-range transport of anthropogenic pollutants to a
477 mountain observatory in east Asia during the 7-SEAS/2010 Dongsha experiment, *Aerosol Air*
478 *Qual. Res.*, 16(11), 2933–2949, <https://doi.org/10.4209/aaqr.2015.07.0440>, 2016.

479 Cheng, F.-Y., Yang, Z.-M., Ou-Yang, C.-F. and Ngan, F.: A numerical study of the dependence
480 of long-range transport of CO to a mountain station in Taiwan on synoptic weather patterns
481 during the Southeast Asia biomass-burning season, *Atmos. Environ.*, 78, 277–290,
482 <https://doi.org/10.1016/j.atmosenv.2013.03.020>, 2013.

483 Cooper, O. R., Gao, R. S., Tarasick, D., Leblanc, T., and Sweeney, C.: Long-term ozone trends at
484 rural ozone monitoring sites across the United States, 1990–2010, *J. Geophys. Res.-*
485 *Atmos.*, 117, 1990–2010, <https://doi.org/10.1029/2012JD018261>, 2012.

486 Deeter, M. N., Edwards, D. P., Francis, G. L., Gille, J. C., Mao, D., Martínez-Alonso, S., Worden,
487 H. M., Ziskin, D., and Andreae, M. O.: Radiance-based retrieval bias mitigation for the
488 MOPITT instrument: the version 8 product, *Atmos. Meas. Tech.*, 12, 4561–4580,
489 <https://doi.org/10.5194/amt-12-4561-2019>, 2019.

490 Doherty, R. M., Stevenson, D. S., Johnson, C. E., Collins, W. J., and Sanderson, M. G.:
491 Tropospheric ozone and El Nino-Southern Oscillation: Influence of atmospheric dynamics,
492 biomass burning emissions, and future climate change, *J. Geophys. Res.*, 111, D19304,
493 <https://doi.org/10.1029/2005JD006849>, 2006.

494 Duncan, B. N., Bey, I., Chin, M., Mickley, L. J., Fairlie, T. D., Martin, R. V., and Matsueda, H.:
495 Indonesian wildfires of 1997: Impact on tropospheric chemistry, *J. Geophys. Res.*, 108, 4458,
496 <https://doi.org/10.1029/2002JD003195>, 2003a.

497 Duncan, B. N., Martin, R. V., Staudt, A., et al.: Inter-annual and seasonal variability of biomass
498 burning emissions constrained by satellite observations, *J. Geophys. Res.*, 108, 4100,
499 <https://doi.org/10.1029/2002JD002378>, 2003b.

500 Field, R. D., van der Werf, G. R., and Shen, S. S. P.: Human amplification of drought-induced
501 biomass burning in Indonesia since 1960, *Nature Geoscience*, 2, 185–188,
502 <https://doi.org/10.1038/ngeo443>, 2009.

503 Field, R. D., van der Werf, G. R., Fanin, T., Fetzer, E. J., Fuller, R., Jethva, H., Levy, R., Livesey,
504 N. J., Luo, M., Torres, O., and Worden, H. M.: Indonesian fire activity and smoke pollution in
505 2015 show persistent nonlinear sensitivity to El Niño-induced drought, *Proceedings of the*
506 *National Academy of Sciences*, 113, 9204–9209, <https://doi.org/10.1073/pnas.1524888113>,
507 2016.

508 Gelaro, R., McCarty, W., Suárez, M. J., Todling, R., Molod, A., Takacs, L., Randles, C. A.,
509 Darmenov, A., Bosilovich, M. G., Reichle, R., Wargan, K., Coy, L., Cullather, R., Draper, C.,
510 Akella, S., Buchard, V., Conaty, A., Silva, A. M. da, Gu, W., Kim, G.-K., Koster, R., Lucchesi,
511 R., Merkova, D., Nielsen, J. E., Partyka, G., Pawson, S., Putman, W., Rienecker, M., Schubert,
512 S. D., Sienkiewicz, M., and Zhao, B.: The Modern-Era Retrospective Analysis for Research
513 and Applications, Version 2 (MERRA-2), *J. Climate*, 30, 5419–5454,
514 <https://doi.org/10.1175/jcli-d-16-0758.1>, 2017.

515 Giglio, L., Schroeder, W., and Justice, C. O.: The collection 6 MODIS active fire detection
516 algorithm and fire products, *Remote Sens. Environ.*, 178, 31–41,
517 <https://doi.org/10.1016/j.rse.2016.02.054>, 2016.

518 Hadley, G.: Concerning the cause of the general trade-winds. *Philos. Trans. R. Soc. Lond.* 29, 58–
519 62. <https://doi.org/10.1098/rstl.1735.0014>, 1735.

520 Heymann, J., Reuter, M., Buchwitz, M., Schneising, O., Bovensmann, H., Burrows, J. P., Massart,
521 S., Kaiser, J. W., and Crisp, D.: CO₂ emission of Indonesian fires in 2015 estimated from
522 satellite-derived atmospheric CO₂ concentrations, *Geophys. Res. Lett.*, 44, 1537–1544,
523 <https://doi.org/10.1002/2016gl072042>, 2017.

524 Hsiao, T. C., Ye, W. C., Wang, S. H., Tsay, S. C., Chen, W. N., Lin, N. H., Lee, C. Te, Hung, H.
525 M., Chuang, M. T., and Chantara, S.: Investigation of the CCN activity, BC and UVBC mass
526 concentrations of biomass burning aerosols during the 2013 BASELInE campaign, *Aerosol Air*
527 *Qual. Res.*, 16, 2742–2756, <https://doi.org/10.4209/aaqr.2015.07.0447>, 2016.

528 Huang, L., Lin, W., Li, F., Wang, Y. and Jiang, B.: Climate Impacts of the Biomass Burning in
529 Indochina on Atmospheric Conditions over Southern China. *Aerosol Air Qual. Res.* 19: 2707-
530 2720. <https://doi.org/10.4209/aaqr.2019.01.0028>, 2019.

531 Huang, H. Y., Wang, S. H., Huang, W. X., Lin, N. H., Chuang, M. T., da Silva, A. M. and Peng,
532 C. M.: Influence of Synoptic-Dynamic Meteorology on the Long-Range Transport of Indochina
533 Biomass Burning Aerosols, *J. Geophys. Res. Atmos.*, 125(3),
534 <https://doi.org/10.1029/2019JD031260>, 2020.

535 Huijnen, V., Wooster, M. J., Kaiser, J. W., Gaveau, D. L. A., Flemming, J., Parrington, M., Inness,
536 A., Murdiyarsa, D., Main, B., and van Weele, M.: Fire carbon emissions over maritime
537 southeast Asia in 2015 largest since 1997, *Sci. Rep.*, 6, 26886,
538 <https://doi.org/10.1038/srep26886>, 2016.

539 Lin, C.-Y., Hsu, H.-m., Lee, Y. H., Kuo, C. H., Sheng, Y.-F., and Chu, D. A.: A new transport
540 mechanism of biomass burning from Indochina as identified by modeling studies, *Atmos.*
541 *Chem. Phys.*, 9, 7901–7911, <https://doi.org/10.5194/acp-9-7901-2009>, 2009.

542 Lin, N.-H., Tsay, S.-C., Maring, H. B., Yen, M.-C., Sheu, G.-R., Wang, S.-H., Chi, K. H., Chuang,
543 M.-T., Ou-Yang, C.-F., Fu, J. S., Reid, J. S., Lee, C.-T., Wang, L.-C., Wang, J.-L., Hsu, C. N.,
544 Sayer, A. M., Holben, B. N., Chu, Y.-C., Nguyen, X. A., Sopajaree, K., Chen, S.-J., Cheng, M.-
545 T., Tsuang, B.-J., Tsai, C.-J., Peng, C.-M., Schnell, R. C., Conway, T., Chang, C.-T., Lin, K.-
546 S., Tsai, Y. I., Lee, W.-J., Chang, S.-C., Liu, J.-J., Chiang, W.-L., Huang, S.-J., Lin, T.-H. and
547 Liu, G.-R.: An overview of regional experiments on biomass burning aerosols and related
548 pollutants in Southeast Asia: From BASE-ASIA and the Dongsha Experiment to 7-SEAS,
549 *Atmos. Environ.*, 78, 1–19, <https://doi.org/10.1016/j.atmosenv.2013.04.066>, 2013.

550 Lin, C. C., Chen, W. N., Loftus, A. M., Lin, C. Y., Fu, Y. T., Peng, C. M. and Yen, M. C.:
551 Influences of the long-range transport of biomass-burning pollutants on surface air quality

552 during 7-SEAS field campaigns, *Aerosol Air Qual. Res.*, 17(10), 2595–2607,
553 <https://doi.org/10.4209/aaqr.2017.08.0273>, 2017.

554 Logan, J. A., Megretskaia, I., Nassar, R., Murray, L. T., Zhang, L., Bowman, K. W., Worden, H.
555 M., and Luo, M.: Effects of the 2006 El Niño on tropospheric composition as revealed by data
556 from the Tropospheric Emission Spectrometer (TES), *Geophys. Res. Lett.*, 35, 1–5,
557 <https://doi.org/10.1029/2007GL031698>, 2008.

558 Matsueda, H. and Inoue, H. Y.: Aircraft measurements of trace gases between Japan and Singapore
559 in October of 1993, 1996, and 1997, *Geophys. Res. Lett.*, 26, 2413–2416,
560 <https://doi.org/10.1029/1999GL900089>, 1999.

561 Matsueda, H., Inoue, H. Y., and Ishii, M.: Aircraft observation of carbon dioxide at 8–13 km
562 altitude over the western Pacific from 1993 to 1999, *Tellus B*, 54, 1–21,
563 <https://doi.org/10.1034/j.1600-0889.2002.00304.x>, 2002.

564 Matsueda, H., Buchholz, R. R., Ishijima, K., Worden, H. M., Hammerling, D., and Machida, T.:
565 Interannual Variation of Upper Tropospheric CO over the Western Pacific Linked with
566 Indonesian Fires, *SOLA*, 15, 205–210, <https://doi.org/10.2151/sola.2019-037>, 2019.

567 Nara, H., Tanimoto, H., Nojiri, Y., Mukai, H., Zeng, J., Tohjima, Y., and Machida, T.: CO
568 emissions from biomass burning in South-east Asia in the 2006 El Niño year: shipboard and
569 AIRS satellite observations, *Environ. Chem.*, 8, 213–223, <https://doi.org/10.1071/EN10113>,
570 2011.

571 Nassar, R., Logan, J. A., Megretskaia, I. A., Murray, L. T., Zhang, L., and Jones, D. B. A.: Analysis
572 of tropical tropospheric ozone, carbon monoxide, and water vapor during the 2006 El Niño
573 using TES observations and the GEOS Chem model, *J. Geophys. Res.-Atmos.*, 114, D17304,
574 <https://doi.org/10.1029/2009JD011760>, 2009.

575 Niwa, Y., Sawa, Y., Nara, H., Machida, T., Matsueda, H., Umezawa, T., Ito, A., Nakaoka, S.-I.,
576 Tanimoto, H., and Tohjima, Y.: Estimation of fire-induced carbon emissions from Equatorial
577 Asia in 2015 using in situ aircraft and ship observations, *Atmos. Chem. Phys.*, 21, 9455–9473,
578 <https://doi.org/10.5194/acp-21-9455-2021>, 2021.

579 Ou-Yang, C. F., Lin, N. H., Lin, C. C., Wang, S. H., Sheu, G. R., Lee, C. Te, Schnell, R. C., Lang,
580 P. M., Kawasato, T. and Wang, J. L.: Characteristics of atmospheric carbon monoxide at a high-
581 mountain background station in East Asia, *Atmos. Environ.*, 89, 613–622,
582 <https://doi.org/10.1016/j.atmosenv.2014.02.060>, 2014.

583 Ou-Yang, C. F., Ravindra Babu, S., Jia-Ren Lee, Ming-Cheng Yen, Stephen M. Griffith, Chia-
584 Ching Lin, Shuenn-Chin Chang and Neng-Huei Lin.: Detection of stratospheric intrusion events
585 and their role in ozone enhancement at a mountain background site in sub-tropical East Asia,
586 *Atmos. Environ.*, 268, 118779, <https://doi.org/10.1016/j.atmosenv.2021.118779>, 2022.

587 Pani, S. K., Wang, S. H., Lin, N. H., Lee, C. Te, Tsay, S. C., Holben, B. N., Janjai, S., Hsiao, T.
588 C., Chuang, M. T. and Chantara, S.: Radiative effect of springtime biomass-burning aerosols
589 over northern Indochina during 7-SEAS/BASELInE 2013 campaign, *Aerosol Air Qual. Res.*,
590 16(11), 2802–2817, <https://doi.org/10.4209/aaqr.2016.03.0130>, 2016.

591 Pani, S. K., Ou-Yang, C.-F., Wang, S.-H., Ogren, J. A., Sheridan, P. J., Sheu, G.-R., and Lin, N.-
592 H. J. A. E.: Relationship between long-range transported atmospheric black carbon and carbon
593 monoxide at a high-altitude background station in East Asia, *Atmos. Environ.*, 210, 86-99,
594 <https://doi.org/10.1016/j.atmosenv.2019.04.053>, 2019.

595 Pan, X., Chin, M., Ichoku, C. M., and Field, R. D.: Connecting Indonesian fires and drought with
596 the type of El Niño and phase of the Indian Ocean dipole during 1979–2016, *J. Geophys. Res.-*
597 *Atmos.*, 123, 1–15, <https://doi.org/10.1029/2018JD028402>, 2018.

598 Park, S., Kim, S.W., Lin, N.H., Pani, S.K., Sheridan, P.J. and Andrews, E.: Variability of Aerosol
599 Optical Properties Observed at a Polluted Marine (Gosan, Korea) and a High-altitude Mountain
600 (Lulin, Taiwan) Site in the Asian Continental Outflow. *Aerosol Air Qual. Res.* 19: 1272-1283.
601 <https://doi.org/10.4209/aaqr.2018.11.0416>, 2019.

602 Parker, R. J., Boesch, H., Wooster, M. J., Moore, D. P., Webb, A. J., Gaveau, D., and Murdiyarso,
603 D.: Atmospheric CH₄ and CO₂ enhancements and biomass burning emission ratios derived
604 from satellite observations of the 2015 Indonesian fire plumes, *Atmos. Chem. Phys.*, 16, 10111–
605 10131, <https://doi.org/10.5194/acp-16-10111-2016>, 2016.

606 Pochanart, P., Akimoto, H., Kajii, Y., and Sukasem, P.: Carbon monoxide, regional-scale, and
607 biomass burning in tropical continental Southeast Asia: Observations in rural Thailand, *J.*
608 *Geophys. Res.-Atmos.*, 108, 4552, <https://doi.org/10.1029/2002JD003360>, 2003.

609 Ravindra Babu, S., VenkataRatnam, M., Basha, G., Liou, Y.-A., and Narendra Reddy, N.: Large
610 Anomalies in the Tropical Upper Troposphere Lower Stratosphere (UTLS) Trace Gases
611 Observed during the Extreme 2015–16 El Niño Event by Using Satellite Measurements,
612 *Remote Sensing*, 11, 687, <https://doi.org/10.3390/rs11060687>, 2019.

613 Ravindra Babu, S. and Liou, Y. A.: Tropical tropopause layer evolution during 2015–16 El Niño
614 event inferred from COSMIC RO measurements, *J. Atmos. Sol.-Terr. Phys.*, 212, 105507,
615 <https://doi.org/10.1016/j.jastp.2020.105507>, 2021.

616 Ravindra Babu, S., Venkat Ratnam, M., Basha, G., Pani, S. K., and Lin, N.-H.: Structure,
617 dynamics, and trace gas variability within the Asian summer monsoon anticyclone in the
618 extreme El Niño of 2015–2016, *Atmos. Chem. Phys.*, 21, 5533–5547,
619 <https://doi.org/10.5194/acp-21-5533-2021>, 2021.

620 Ravindra Babu, S., Nguyen, L. S. P., Sheu, G.-R., Griffith, S. M., Pani, S. K., Huang, H.-Y., and
621 Lin, N.-H.: Long-range transport of La Soufrière volcanic plume to the western North Pacific:
622 Influence on atmospheric mercury and aerosol properties, *Atmos. Environ.*, 268, 118806,
623 <https://doi.org/10.1016/j.atmosenv.2021.118806>, 2022a.

624 Ravindra Babu, S., Pani, S.K., Ou-Yang, C.F., Lin, N.H.: Impact of 21 June 2020 Annular Solar
625 Eclipse on Meteorological Parameters, O₃ and CO at a High Mountain Site in Taiwan. *Aerosol*
626 *Air Qual. Res.* 22, 220248. <https://doi.org/10.4209/aaqr.220248>, 2022b.

627 Reid, J. S., Hyer, E. J., Johnson, R., Holben, B. N., Yokelson, R. J., Zhang, J., Campbell, J. R.,
628 Christopher, S. A., Di Girolamo, L., Giglio, L., Holz, R. E., Kearney, C., Miettinen, J., Reid,
629 E. A., Turk, F. J., Wang, J., Xian, P., Zhao, G., Balasubramanian, R., Chew, B. N., Janai, S.,
630 Lagrosas, N., Lestari, P., Lin, N.-H., Mahmud, M., Nguyen, A. X., Norris, B., Oahn, N. T. K.,
631 Oo, M., Salinas, S. V., Welton, E. J., Liew, S. C.: Observing and understanding the Southeast
632 Asian aerosol system by remote sensing: An initial review and analysis for the Seven Southeast
633 Asian Studies (7SEAS) program, *Atmos. Res.*, 122, 403-468,
634 <https://doi.org/10.1016/j.atmosres.2012.06.005>, 2013.

635 Sheu, G.-R., Lin, N.-H., Wang, J.-L., Lee, C.-T.; Lulin Atmospheric Background Station: A New
636 High-Elevation Baseline Station in Taiwan, *J-STAGE*, Volume 24, Issue 2, Pages 84-89,
637 <https://doi.org/10.11203/jar.24.84>, 2009.

638 Tsay, S. C., Maring, H. B., Lin, N. H., Buntoung, S., Chantara, S., Chuang, H. C., Gabriel, P. M.,
639 Goodloe, C. S., Holben, B. N., Hsiao, T. C., Christina Hsu, N., Janjai, S., Lau, W. K. M., Lee,
640 C. Te, Lee, J., Loftus, A. M., Nguyen, A. X., Nguyen, C. M., Pani, S. K., Pantina, P., Sayer, A.
641 M., Tao, W. K., Wang, S. H., Welton, E. J., Wiriya, W. and Yen, M. C.: Satellitesurface
642 perspectives of air quality and aerosol-cloud effects on the environment: An overview of 7-
643 SEAS/BASELInE, *Aerosol Air Qual. Res.*, 16(11), 2581–2602,
644 <https://doi.org/10.4209/aaqr.2016.08.0350>, 2016.

645 van der Werf, G. R., Dempewolf, J., Trigg, S. N., Randerson, J. T., Kasibhatla, P. S., Giglio, L.,
646 Murdiyarso, D., Peters, W., Morton, D. C., Collatz, G. J., Dolman, A. J., and DeFries, R. S.:
647 Climate regulation of fire emissions and deforestation in equatorial Asia, *Proc. Natl. Acad. Sci.*
648 *USA*, 105, 20350–20355, <https://doi.org/10.1073/pnas.0803375105>, 2008.

649 van der Werf, G. R., Randerson, J. T., Giglio, L., van Leeuwen, T. T., Chen, Y., Rogers, B. M.,
650 Mu, M., van Marle, M. J. E., Morton, D. C., Collatz, G. J., Yokelson, R. J., and Kasibhatla, P.
651 S.: Global fire emissions estimates during 1997–2016, *Earth Syst. Sci. Data*, 9, 697–720,
652 <https://doi.org/10.5194/essd-9-697-2017>, 2017.

653 Wang, C.: ENSO, Atlantic climate variability, and the Walker and Hadley circulations, in: *The*
654 *Hadley circulation: Present, past and future*, Springer, Berlin, 173–202,
655 https://doi.org/10.1007/978-1-4020-2944-8_7, 2004.

656 Wang, S.-H., Welton, E. J., Holben, B. N., Tsay, S.-C., Lin, N.-H., Giles, D., Stewart, S. A., Janjai,
657 S., Nguyen, X. A., Hsiao, T.-C., Chen, W.-N., Lin, T.-H., Buntoung, S., Chantara, S., and
658 Wiriya, W.: Vertical Distribution and Columnar Optical Properties of Springtime Biomass-
659 Burning Aerosols over Northern Indochina during 2014 7-SEAS Campaign, *Aerosol Air Qual.*
660 *Res.*, 15, 2037–2050, <https://doi.org/10.4209/aaqr.2015.05.0310>, 2015.

661 Weng, H. Y., Behera, S. K., and Yamagata, T.: Anomalous winter climate conditions in the Pacific
662 rim during recent El Niño Modoki and El Niño events, *Clim. Dynam.*, 32, 663–674,
663 <https://doi.org/10.1007/s00382-008-0394-6>, 2009.

664 Whitburn, S., Van Damme, M., Clarisse, L., Turquety, S., Clerbaux, C., and Coheur, P.-F.:
665 Doubling of annual ammonia emissions from the peat fires in Indonesia during the 2015 El
666 Niño, *Geophys. Res. Lett.*, 43, 11007–11014, <https://doi.org/10.1002/2016gl070620>, 2016.

667 Worden, J., Jiang, Z., Jones, D. B. A., Alvarado, M., Bowman, K., Frankenberg, C., Kort, E. A.,
668 Kulawik, S. S., Lee, M., Liu, J., Payne, V., Wecht, K., and Worden, H.: El Niño, the 2006
669 Indonesian peat fires, and the distribution of atmospheric methane, *Geophys. Res. Lett.*, 40,
670 4938–4943, <https://doi.org/10.1002/grl.50937>, 2013.

671 Yin, Y., Ciais, P., Chevallier, F., van der Werf, G. R., Fanin, T., Broquet, G., Boesch, H., Cozic,
672 A., Hauglustaine, D., Szopa, S., and Wang, Y.: Variability of fire carbon emissions in equatorial
673 Asia and its nonlinear sensitivity to El Niño, *Geophys. Res. Lett.*, 43, 10472–10479,
674 <https://doi.org/10.1002/2016gl070971>, 2016.

675

676 **Table 1.** Detailed statistics of observed CO in October during 2006 to 2021 at LABS.

Year	Mean	Median	Standard Deviation	CO anomalies (ppb)	Change in CO (%)	Total data points
2006	175.8	174	51	47.2	37.2	703
2007	155.3	140	63.4	13.2	10.41	732
2008	125.5	125	26.9	-1.8	-1.42	599
2009	127.1	125	35.5	-1.8	-1.42	533
2010	143.9	136	38.1	9.2	7.2	739
2011	137.1	137	41.9	10.2	8.0	734
2012	155.8	153	39.4	26.2	20.6	643
2013	146.8	141	35.7	14.2	11.2	365
2014	125.6	120	39.8	-6.8	-5.4	602
2015	164.8	163.5	46.2	36.7	28.9	732
2016	91.6	87	20.9	-39.8	-31.4	732
2017	109.7	100.3	32.4	-26.5	-20.9	744
2018	147.7	149.9	29.1	23.1	18.2	736
2019	142.4	142.8	37.7	16	12.6	742
2020	121.3	113.8	29.5	-13	-10.2	742
2021	107.7	104.6	26.9	-22.2	-17.5	744

677